J. COMBIN. MATH. COMBIN. COMPUT. 127b (2025) 3753--3769

Journal of Combinatorial Mathematics and Combinatorial Computing
www.combinatorialpress.com/jcmcc

Numerical simulation of heat transfer characteristics of high temperature devices based on nonlinear partial differential equations

Yan Zhang[1,✉], Ruchuan Shi[2]

[1] *School of Information Engineering, Nanyang Institute of Technology, Nanyang, Henan, 473004, China*
[2] *College of Perception Science and Engineering, Shanghai Jiaotong University, Shanghai, 200240, China*

ABSTRACT
This study takes the physical properties of high temperature devices as a starting point and the experimental apparatus used to obtain the study samples. The heat transfer process can be categorized into heat conduction, heat convection and heat radiation depending on the mode of contact. Under the theoretical support of the first law of thermodynamics, the nonlinear partial differential equations of the heat transfer characteristics of the high temperature devices are determined, and the above equations are analyzed by numerical simulation with the help of ANSYS software. When the thickness of the device is 1um, 8um and 15um, the heat transfer temperature and the power of the heat source show a monotonically increasing trend, in addition, when the thickness of the device is a fixed value, the spacing of the heat source and the heat transfer temperature show a nonlinear monotonically decreasing, and the present study has an important practical significance for improving the heat transfer performance of high temperature devices.

Keywords: nonlinear partial differentiation, ANSYS software, high temperature devices, heat transfer, numerical simulation

1. Introduction

Heat transfer problems are important in many practical applications, such as materials science, engineering thermodynamics, and geology. Among these problems, the heat conduction equation is a key mathematical model that describes the temperature distribution and heat transfer process in a substance. The study of modeling heat transfer problems based on partial differential equations aims to investigate the heat transfer process through mathematical methods and computational simulations in order to solve practical problems and optimize designs [1-4].

✉ Corresponding author.
E-mail address: Meihaozhilu_2025@163.com (Y. Zhang).
Received 25 October 2024; Revised 10 December 2024; Accepted 05 March 2025; Published Online 16 April 2025.
DOI: 10.61091/jcmcc127b-209

With the increasing integration of electronic devices and their increasing power density, they face more and more serious thermal failure problems. High temperatures can cause electronic devices to suffer from solder joint fatigue, solder joint detachment, dielectric film fracture, chip fracture and other problems, leading to the performance degradation or even failure of electronic devices, and a significant reduction in their lifespan [5-8]. High temperature is an important factor restricting the development of electronic devices, so the thermal management of electronic devices has become increasingly important. The heat dissipation technology of electronic devices under room temperature conditions is relatively mature, and its basic principle is to transfer the self-generated heat of electronic devices to the environment through heat conduction, convection or radiation heat transfer [9-12]. On the contrary, for extreme occasions with high ambient temperatures, such as oil logging, aerospace, and military fields, where the external ambient temperature is higher than the temperature of the electronic device, the self-generated heat of the electronic device can not be distributed to the environment, and the high-temperature environment accelerates the temperature rise of the electronic device instead [13-16]. Therefore, numerical simulation of device heat transfer characteristics using nonlinear partial differential equations plays an important role in exploiting the performance of electronic devices.

The article takes the physical characteristics and structure of high-temperature devices as the starting point, builds the experimental environment, collects and makes the high-temperature device samples. Based on the different modes of action of the high-temperature device, the heat transfer process of the high-temperature device can be divided into three modes: heat conduction, heat convection and heat radiation. Under the constraints of the principle of energy conservation, the nonlinear partial differential equations of the heat transfer characteristics of the high-temperature device are obtained by using mathematical methods such as mathematical derivation and differentiation. In order to better visualize the heat transfer characteristics of the sample, the corresponding numerical simulation scheme is formulated, and the heat transfer characteristics of the high-temperature device are simulated and analyzed by numerical simulation using ANSYS software, which is of guiding value for improving the thermodynamic performance of the high-temperature device.

2. Nonlinear partial differential equations and numerical simulation software

2.1. Nonlinear partial differential equations

Nonlinear dynamics belongs to the category of nonlinear science, and many processes of nonlinear dynamics can be formulated using nonlinear partial differential equations (sets), therefore, the problem of solving the nonlinear partial differential equations has been the focus of research in various fields [17-18]. The earliest nonlinear partial differential equations were established by DJKorteweg and GDeVries of the University of Amsterdam, the Netherlands, in their study of the equations of motion of shallow water waves;

$$\frac{\partial u}{\partial t}-6u\frac{\partial u}{\partial x}+\frac{\partial^3 u}{\partial x^3}=0 \tag{1}$$

This equation is the famous KdV equation. Since this equation was proposed, many other nonlinear partial differential equations, such as the Burgers equation, the KdV-Burgers equation, the N-S equation, and so on, have been proposed based on a variety of physical and engineering practical problems.

Once the nonlinear partial differential equations describing various nonlinear dynamics are proposed, the research on the exact or approximate solution of nonlinear partial differential equations in computer science, mathematics, physics and other disciplines has never stopped [19]. After decades of development, many methods for solving nonlinear partial differential equations have been proposed, such as: backscattering method, bilinear transformation method, separated variable method, etc. In computational fluid dynamics, the method of solving nonlinear partial differential equations is often used to solve nonlinear partial differential equations. In computational fluid dynamics, nonlinear partial differential equation solution studies are often carried out by using discretization methods (finite element method, finite difference method, finite volume method, etc.). In recent years, thanks to the rapid development of machine learning technology, especially the neural network technology in deep learning, the use of neural networks powerful nonlinear modeling ability to study the approximate solution of nonlinear partial differential equations is also favored by researchers.

The purely data-driven approximate solution method draws entirely on the nonlinear modeling capabilities of neural networks, which do not provide the neural network model with any physical a priori knowledge, but rather allow the model to uncover and learn the relevant information from the training samples completely independently, which allows the network model to be a good substitute for nonlinear partial differential equations to give predictive solutions for the quantities of interest. As far as the method itself is concerned, it is not different from the general training method of neural networks. So by the basic theory of neural network modeling, for the regression problem, the method selects the mean squared loss function for the multidimensional dataset:

$$loss = \frac{1}{2N}\sum_{i=1}^{N}\left\| y_i - f(x_i)\right\|_2^2 \tag{2}$$

In this paper, the method is improved by having a mapping relationship between the inputs as well as the outputs of the model that can be described by a nonlinear partial differential equation, for the fluid problem.

Finally, the update of the network model parameters, weights matrix W and bias vectors b is performed using the error back propagation algorithm:

$$(W,b) = \arg\min_{W,b}(loss) \tag{3}$$

Aiming at the existing problems such as the lack of physical interpretability in the pure data-driven approximate solution method, and the coupled a priori knowledge of the neural network model a priori knowledge is too single and simple, on the basis of the pure data-driven method, due to the existence of mapping relationship between the model inputs as well as the outputs, a neural network model of the coupled nonlinear partial differential equations is proposed, and the unnecessary assumptions in the coupling process are removed, so as to simplify the coupling process. simplification. Consider nonlinear partial differential equations:

$$\Omega(x(x^1,x^2,\cdots,x^{n-1},x^n), y(y^1,y^2,\cdots,y^{n-1},y^n)); (\theta_1,\theta_2,\cdots,\theta_{n-1},\theta_n)) = 0 \tag{4}$$

where $x(x^1,x^2,\cdots,x^{n-1},x^n), y(y^1,y^2,\cdots,y^{n-1},y^n)$ denotes physical quantities associated with nonlinear partial differential equations, such as coordinates, time, velocity, pressure, etc. in computational fluid dynamics, which are separated because one part of the physical quantities $x(x^1,x^2,\ldots,x^{n-1},x^n)$ is used as an input to the neural network model and the other part of the quantities $y(y^1,y^2,\ldots,y^{x-1},y^x)$ is used as an output of the model. Then:

$$(\theta_1,\theta_2,\ldots,\theta_{s-1},\theta_s) \tag{5}$$

represents the coefficients in the nonlinear partial differential equation.

Since in the purely data-driven approach we have $f(x_i)$ as the predicted output of the neural network model, the nonlinear partial differential equation can be re-represented using the input physical quantities of the model and $f(x_i)$, thus defining the auxiliary function h:

$$h = \Omega(x(x^1, x^2, \cdots, x^{n-1}, x^n), f(x)); (\theta_1, \theta_2, \cdots, \theta_{n-1}, \theta_n)) \tag{6}$$

Our solution goal is to use the neural network model to find $x(x^1, x^2, \cdots, x^{n-1}, x^n), y(y^i, y^2, \cdots, y^{n-1}, y^n)$ so that Eq. (6) holds, and Eq. (7) happens to be the bridge between the neural network model and the nonlinear partial differential equation, then the approximate solution of the nonlinear partial differential equation can be found by constantly converging h to zero through the output value $f(x_i)$ of the neural network:

$$h = \Omega(x(x^1, x^2, \cdots, x^{n-1}, x^n), f(x)); (\theta_1, \theta_2, \cdots, \theta_{n-1}, \theta_n)) \to 0 \tag{7}$$

The question now is how to represent Eq. (7) with in the neural network model. Considering the early use of neural networks in conjunction with traditional methods, it is possible to couple the nonlinear partial differential equations in the loss function of the neural network model. Specifically, a loss term with respect to h^2 minimization is added to the purely data-driven neural network approach mean-variance loss function:

$$loss_{total} = loss + loss_k = \frac{1}{2N}\sum_{i=1}^{N}\|y_i - f(x_i)\|_2^2 + \frac{1}{2N}\sum_{i=1}^{N} h_i^2 \tag{8}$$

For many nonlinear problems, the process often does not have a single nonlinear partial differential equation. Thus for a process containing a system of equations with M nonlinear partial differential equation, Eq. (9) is expressed as using Eq. (8) below:

$$loss_{total} = loss + \sum_{j=1}^{M} loss_{k'} = \frac{1}{2N}\sum_{i=1}^{N}\|y_i - f(x_i)\|_2^2 + \frac{1}{2N}\sum_{j=1}^{M}\sum_{i=1}^{N}(h_i^j)^2 \tag{9}$$

Similarly, the update of the network model parameters, weight matrix W and bias vector b, is performed using the error back propagation algorithm:

$$(W, b) = \arg\min_{W,b}(loss_{tosal}) \tag{10}$$

2.2. Numerical simulation software

In analogy with related numerical simulation software, the main features of ANSYS software are:

1) It is easy to use because ANSYS is a Windows program.

2) It can be applied in various projects because the software framework of ANSYS is synthesized by various complete modules.

3) Not only can the structure be solved linearly, but also many kinds of nonlinear examples can be analyzed.

4) Not only can the direction of molecular heat transfer in high temperature devices be studied independently, but also the interaction between them can be studied.

ANSYS software can analyze most of the heat transfer and related projects in scientific research. Through the use of ANSYS process can be summarized finite element analysis into three steps: first, first pre-processing, mainly contains the definition of the type, set the properties, draw the model, sub-network and other work [20-21]. The second is the solution, which mainly contains the work of adding constraints, increasing loads, observing the wrong solution, and finding out the results, etc. The third is the post-processing. The third is post-processing, which mainly contains work such as listing results, drawing graphs, displaying animations, drawing conclusions, etc.

3. Characterization of heat transfer in high-temperature devices

3.1. High temperature device structure and preparation

3.1.1. Device Structure. High-temperature devices are, in descending order, the substrate, the AlN nucleation layer, the gallium nitride buffer layer, the AlGaN barrier layer, the passivation layer, and the electrodes. The substrate for high temperature devices is usually sapphire or silicon carbide. Sapphire and gallium nitride have the same crystal structure, so in the sapphire epitaxial growth of gallium nitride crystal quality is higher, and sapphire cost is low, easy to industrialize the large-scale production, but the thermal conductivity is low, not conducive to the device through the substrate heat dissipation, in the field of high-power applications will produce a serious self-heating effect. Silicon carbide thermal conductivity than sapphire is high, conducive to device heat dissipation, but also has good electrical properties, convenient for device packaging substrate grounding, however, silicon carbide and gallium nitride there is a large lattice mismatch, which will affect the crystal quality of the buffer layer, and the production is difficult, high manufacturing costs.

AlN nucleation layer thickness is generally 2 ~ 3nm, the role of the release of thermal stress between the two material layers, gallium nitride crystal lateral growth, in order to reduce the lattice mismatch, to improve the growth quality of GaN crystal. At the same time, AlN also exists to separate the role of the substrate and gallium nitride, to prevent different materials from diffusing each other.

The GaN buffer layer will inevitably introduce N-type background carriers during epitaxial growth, so the buffer layer is N-type GaN. However, when the buffer layer is subjected to high voltage, the introduced background carriers will seriously affect the breakdown voltage of the device, so the preparation process is generally Fe-doped or C-doped for the buffer layer to deplete the background carriers. The structural parameters of the barrier layer material determine the 2DEG performance, and thus the Al component and thickness can neither be high nor low, and in general the Al component is 25%~35% and the thickness is 18nm~35nm.

The gate of the device forms a Schottky contact with the semiconductor, and by applying different gate voltages, the density of the channel 2DEG underneath it is controlled, which in turn enables the switching of the conducting channel, as well as the control of the current density during conduction. The source and drain contacts with the heterojunction semiconductor form ohmic contacts. When the conductive channel is on, a voltage is applied to the source and drain to generate a transverse electric field in the channel, and the 2DEG drifts in response to the electric field, resulting in the formation of a current path.

3.1.2. High temperature device preparation. The high-temperature devices used in this experiment were obtained from the State Key Laboratory of Wide Bandgap Semiconductor, and the high-temperature device preparation process was as follows:

1) On a sapphire substrate with a crystal orientation of (0001), a 40 nm AIN nucleation layer was grown by metal organic chemical vapor deposition (MOCVD).

2) Growth of 1.5um GaN buffer layer on top of AIN nucleation layer by MOCVD.

3) Epitaxial growth of 20 nm AlGaN layer with 30% aluminum fraction on GaN buffer layer by MOCVD.

4) Deposition of SiN on the AlGaN barrier layer to form a passivation layer using plasma enhanced chemical vapor deposition (PECVD).

5) Firstly, the source and drain regions are defined by semiconductor lithography, secondly, SiN and AlGaN in the electrode region are etched away by ICP process, and finally, four layers of Ti, Al, Ni and Au with thicknesses of 40 nm, 140 nm, 60 nm and 50 nm, respectively, are deposited by electron-beam evaporation and annealed to form the ohmic contact under nitrogen environment at 900℃.

6) The gate electrode region was defined by semiconductor lithography, the passivation layer corresponding to the gate region was etched away by ICP process, and then Ni and Au metal layers

with thicknesses of 53 nm and 520 nm, respectively, were deposited by electron beam evaporation. The GaN buffer layer was Fe doped with a concentration of $2.3x10^{19}cm^{-3}$ in order to deplete the N-type background carriers introduced during epitaxial growth. The gate length Lc of the device is 1um, the gate width WG is 150um, and the distance between source and drain LSD is 8um.

3.2. Heat transfer in high temperature devices

Heat transfer is a method of transferring energy between two different objects, mainly due to the difference in temperature. Heat transfer between objects can be categorized into heat conduction, heat convection and heat radiation.

3.2.1. Heat transfer. Heat conduction occurs when two objects have different temperatures, or when there is a temperature difference between different parts of the same object, and the heat energy is all transferred from the side with the higher temperature to the side with the lower temperature. It is the heat conduction method that is mainly used in the simulations in this chapter. The primary method of heat transfer and transportation within a device is also thermal conduction, which occurs when different parts of the device have temperature changes due to different thermal conductivities, and this heat can be quantified by Fourier's law:

$$Q = \lambda A(T_h - T_1) / \delta \tag{11}$$

where T_h and T_1 are the temperatures of the high and low temperature surfaces in heat transfer, respectively, δ is the distance between the two surfaces, A is the area of the isothermal surface perpendicular to the direction of heat transfer, and λ represents the thermal conductivity of the material.

3.2.2. Thermal convection. Thermal convection occurs mainly in the fluid medium, mainly refers to the exchange of heat between the object and the surrounding fluid medium (such as air, etc.). Mainly includes natural convection heat transfer, forced convection heat transfer and turbulence in three basic forms.

The process of thermal convection conforms to Newton's law of cold removal, and its heat expression is as follows:

$$Q = hA(T_w - T_{ar})\tag{12}$$

3.2.3. Thermal radiation. The radiant energy of an object can be expressed by the Stefan-Boltzmann law as:

$$Q = \sigma \varepsilon A_i F_{ij} (T_i^4 - T_j^4) \tag{13}$$

where σ is the Stephen Boltzmann constant, ε is the object radiation coefficient, A_i is the surface area, F_{ij} is the shape factor from surface i to j, T_i is the absolute temperature of surface i, and T_j denotes the absolute temperature of surface J.

3.3. Nonlinear partial differential equations for heat transfer

According to the principle of conservation of energy, complete heat transfer includes the processes of heat conduction, heat convection and heat radiation. The heat transfer process is the sum of these three modes of heat transfer, which can be expressed in equation (14) as:

$$\overline{\Phi} = -k\nabla \overline{T} + h(T_{m1} - T_{m2}) + \varepsilon_{em}\sigma A_1 F_{12}(T_{m1}^4 - T_{sarjace}^4) \tag{14}$$

Considering the thermal transient process, the thermal conduction process can be expressed in Eq. (15) as:

$$\nabla \cdot (k\nabla \vec{T}) + H = \rho C_p \frac{\partial T}{\partial t} \tag{15}$$

When only the steady state heat transfer is considered, the simplification of Eq. (15) is integrated on both sides to obtain the temperature change in the cross section of the device at power consumption P_{diss} can be expressed in Eq. (16) as;

$$P_{diss} = \frac{T_2 - T_1}{\Delta y / kA} = \frac{\Delta T}{R_{th}} \tag{16}$$

where Δy is the distance in the direction of heat conduction, A is the cross-sectional area, and R_{th} is defined as the thermal resistance of the material that impedes the flow of heat, which is proportional to the thickness of the material, inversely proportional to the thermal conductivity of the material, and inversely proportional to the cross-sectional area A. Equation (16) can be used to calculate the temperature T_{ch} of the channel of a high-temperature device at a specific power consumption and initial reference temperature T_o, which can be expressed in Equation (17) as:

$$T_{ch} = P_{diss} R_{di} + T_0 \tag{17}$$

When transient heat transfer is considered, the dynamics of the channel temperature of a high temperature device can be simplified by Eq. (16) to the following form:

$$P_{diss}(t) = \frac{\Delta T_{ch}}{R_{th}} + C_{th} \frac{d}{dt}(\Delta T_{ch}) \tag{18}$$

From equation (18), it can be seen that R_{th} and C_{th} are two important parameters describing the temperature characteristics of the device channel.

By replacing the instantaneous power consumption $p_{divs}(t)$ and temperature difference ΔT_{ch}, with current source $I_{th}(t)$ and voltage $V_{th}(t)$, respectively, equation (19) can be expressed as:

$$I_{th}(t) = \frac{\Delta V_{th}}{R_{th}} + C_{th} \frac{d}{dt}(\Delta V_{th}) \tag{19}$$

The Fourier transform of equation (20) is done and solved to obtain:

$$\Delta V_{th}(\omega) = H(\omega) R_{th} I_{sh}(\omega) \tag{20}$$

Among them:

$$H(\omega) = \frac{1}{1 + j\omega R_{th} C_{th}} \tag{21}$$

3.4. Numerical simulation program

The numerical simulation method obtains the electro-thermal characteristics of the device by establishing an accurate device model structure and solving the partial differential equations using numerical computation methods, such as finite element and finite time domain difference methods. Numerical simulation method can easily obtain the temperature characteristics inside the device, i.e., in the channel, and overcomes the disadvantages of the analytical method which is difficult to solve and the measurement method which is complicated to test, therefore, in this paper, we adopt the finite element (FEM) method of the commercial numerical simulation software (ANSYS) to analyze the heat transfer characteristics of high-temperature devices. Firstly, it is necessary to establish the model structure of the target, followed by the life of the physical parameters used in the simulation. The structural model is then built into a grid structure, which is divided into a finite number of nonrepeating cells, each of which will include a certain number of nodes. The physical functions are then solved for each cell node. Then set the initial conditions and boundary conditions, according to the law of conservation of energy to solve the partial differential equation of heat transfer at each node, calculate the temperature value of each node, and realize the extraction of the temperature of each place inside the object. The specific process is as follows:

3.4.1. Determination of unit type. There are nearly 200 types of units in ANSYS to choose from, which can meet different types of analysis needs. In this simulation, we choose the 8-node unit related to the analysis of heat transfer characteristics.

3.4.2. Establishment of model dimensions. The simulation model in this case includes a sapphire substrate, a GaN buffer layer, an AlGaN barrier layer, a metal electrode, and a heat source. The generated voxels need to be bonded to form the final model, and the model nodes are reduced for computational simplicity.

3.4.3. Defining Material Layer Properties. Thermal conductivity is very critical in the device junction temperature simulation, so the thermal conductivity of each material layer needs to be selected correctly, after referring to many literatures, the final thermal conductivity used in the simulation is shown in Table 1.

Table 1. The thermal conductivity of each material layer in the device model

Materials	Spphire	GaN	AlGaN	Heat Source	Meatal
Thermal conductivity($W\cdot m^{-1}\cdot k^{-1}$)	$40\left(\frac{300k}{T}\right)$	$130\left(\frac{300k}{T}\right)^{1.4}$	$11\left(\frac{300k}{T}\right)$	$130\left(\frac{300k}{T}\right)^{1.4}$	280

3.4.4. Grid division. The mesh division methods commonly used in ANSYS software generally include mapping division, extension division, liberalization division and adaptive division. Among them, the mapping division can make the model divided into regular shapes, and the calculation accuracy and high speed, which can help the accurate division of the mesh. It is worth noting that mapping requires the mesh to be hexahedral, and irregular models need to be cut in advance.

3.4.5. Applying loads. Firstly, the type of steady state analysis is determined and the boundary conditions are set for the model, in this simulation the bottom surface temperature load is uniformly set to the ambient temperature of 22°C, and the two sides of the device are set to adiabatic conditions. Secondly, the heat flow density is applied to the heat source. When the DC power dissipation of the device is 16W/mm, the corresponding applied heat flow density should be $8\times10^5 W/cm^2$, and the effects of thermal convection and thermal radiation are not considered in this simulation.

3.4.6. Solution Simulation. Through ANSYSY simulation software can be solved in the finite element established in the high temperature device heat transfer characteristics of nonlinear partial differential equations, so as to get the value of the node degrees of freedom, through the numerical simulation of this step can be obtained by the high temperature device heat transfer characteristics of the simulation of the temperature distribution map.

4. Simulation and analysis of heat transfer characteristics of high-temperature devices

4.1. Simulation and analysis of multi-scale heat transfer characteristics of high temperature devices

4.1.1. Device Thickness Impact Analysis. This part aims to explore how the thickness of the GaN layer affects the temperature in the heat transfer of the high temperature device, and the trend of the maximum temperature of the device is analyzed by numerical simulation when the thickness of the GaN layer changes within the range of 1 μm to $10\mu m$. The analysis of the influence of the thickness of the device is shown in Fig. 1, in which (a) ~ (b) are the temperature change curve and the cloud diagram of the temperature distribution, respectively. In the numerical simulation, the bottom boundary condition is set to a constant temperature T=300K, and the rest of the parts are set to adiabatic boundary conditions. It is observed that the maximum temperature of the device shows a trend of decreasing and then increasing with the thickness of the GaN layer. In order to accurately exhibit the maximum temperature at the optimal thickness of GaN layer, the effect of different GaN layer thicknesses on the thermal performance of the device is visualized. With the increase of GaN layer thickness, the maximum temperature of the device first decreases and then increases, especially when the GaN layer thickness reaches 6.13 μm, the lowest maximum temperature is observed. Subsequently, the maximum temperature of the device increases slightly with further increase in the thickness of the GaN layer. This observation is in high agreement with the findings based on the semiclassical phonon transport theory. Therefore, when designing high-temperature devices, analyzing the relationship between the GaN layer thickness and the maximum temperature through numerical simulation can determine the optimal GaN layer thickness, thus effectively reducing the maximum temperature of the device. This provides an efficient and accurate multi-scale thermal analysis tool for the thermal transfer characterization of high-temperature devices, which is an important reference value for the design and fabrication of high-performance related devices.

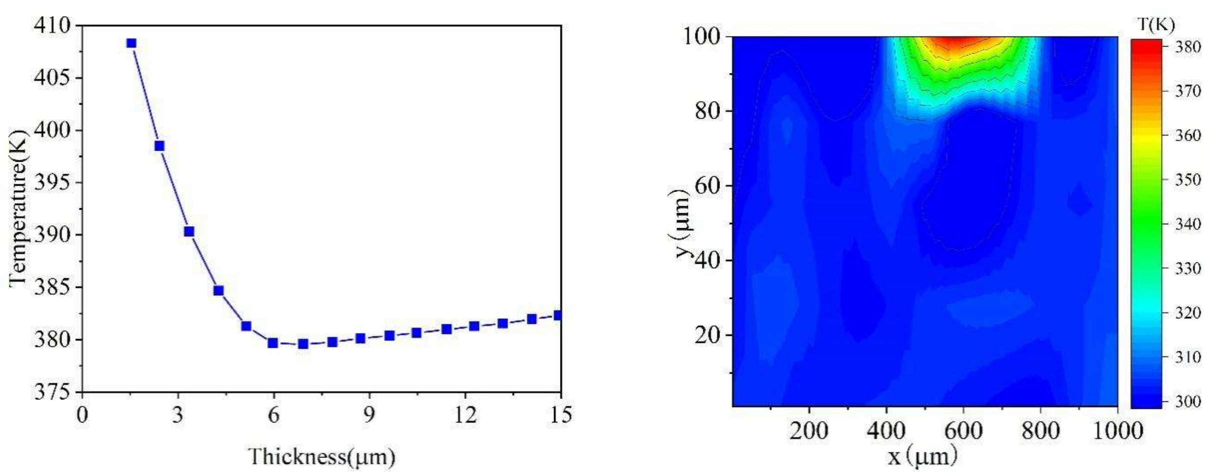

(a)Temperature curve (b)Temperature distribution cloud map

Fig. 1. Influence analysis of device thickness

In addition, three different numerical simulation methods, FDM, LBM and finite element (FEM), are compared in this study in terms of time efficiency and computational accuracy. The results of the computational efficiency and accuracy analysis are shown in Fig. 2, where (a)~(b) are the computational time comparison graph and absolute error comparison, respectively. From Fig. 2(a), it can be clearly observed that the method in this paper significantly improves the computational efficiency by about 33 times under the condition of ensuring equal accuracy with LBM. Further by comparing the computational results with the LBM, Fig. 2(b) demonstrates that the maximum error of this paper's method is no more than 1%, while the maximum error of the conventional macroscopic finite-difference method (FDM) is about 14.6%. This difference indicates that the traditional macroscopic Fourier's law is no longer applicable when the heat source size effect is considered. The method in this paper can effectively capture the size effect of the heat source region while significantly improving the computational efficiency, providing an accurate and efficient numerical simulation tool for complex heat transfer characterization problems.

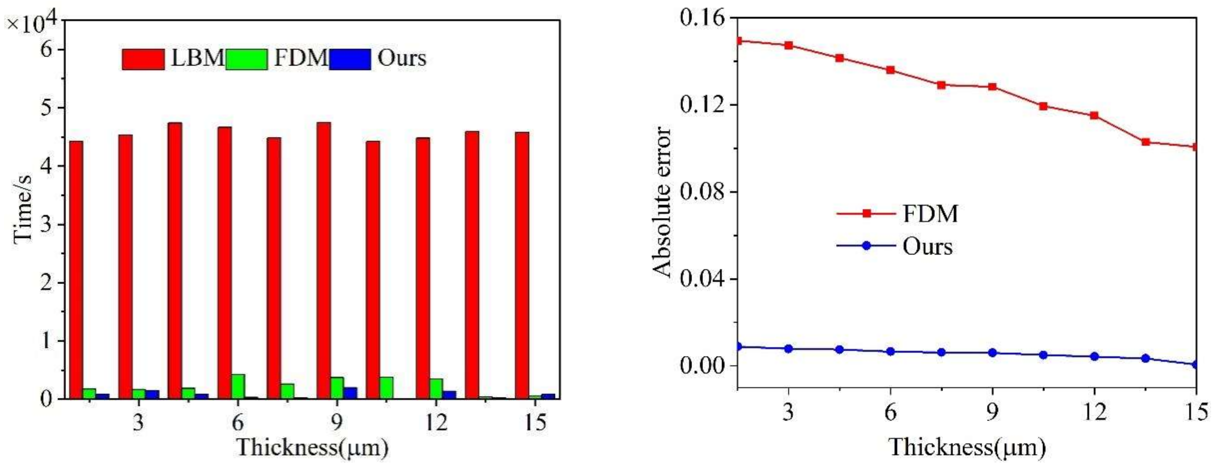

(a)Calculate the time comparison chart (b)Absolute error contrast

Fig. 2. Calculation efficiency and precision analysis results

4.1.2. Heat source power impact analysis. The effect of heat source power on the maximum temperature of three-dimensional integrated circuits and their performance is investigated.In this part, the temperature trend is explored when the heat source power is increased from 10W/mm to 50W/mm by using GaN layer thicknesses of 1um, 8um, and 15um, respectively. Considering that the safe working temperature of electronic devices is generally considered, not exceeding 600 K, therefore, this study depicts the curves of the maximum temperature of the device with the variation of the heat source power as a means of evaluating the effect of thermal analysis at different powers, and the curves of the temperature of the device with the variation of the heat source power are shown in Fig. 3. The device power handling limit under different GaN layer thickness conditions can be calculated by setting the safe operating temperature threshold. Under the assumption that the safe working temperature is set to 1000 K, the maximum power handling limits of the device are 9.05 W/mm, 12.66 W/mm and 10.46 W/mm for GaN layer thicknesses of 1 um, 8 um and 15 um, respectively, and the results further confirm the previous finding that the GaN layer thickness affects the heat transfer characteristics of the device, and the maximum temperature varies with the GaN layer thickness. GaN layer thickness shows a decreasing and then increasing trend.

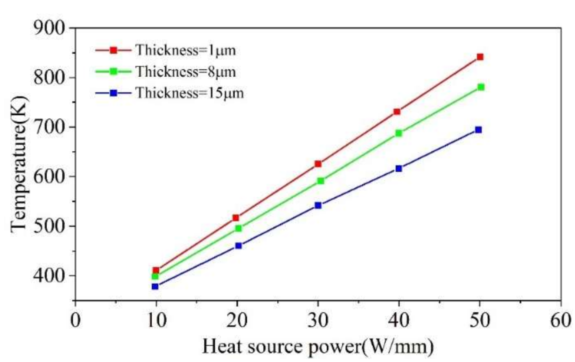

Fig. 3. Device temperature variation curve with heat source power

The temperature distribution of different GaN thicknesses is shown in Fig. 4, where (a) ~ (c) are 1 um, 8 um and 15 um, respectively. it can be seen that as the thickness of the GaN layer decreases, the heat is concentrated near the heat source, which leads to an increase in the local temperature. Whereas, the increase in the thickness of the GaN layer promotes the lateral diffusion of heat within the layer, which helps to reduce the local temperature gradient and achieve a more uniform temperature distribution, which is essential for improving the reliability and performance of the device.

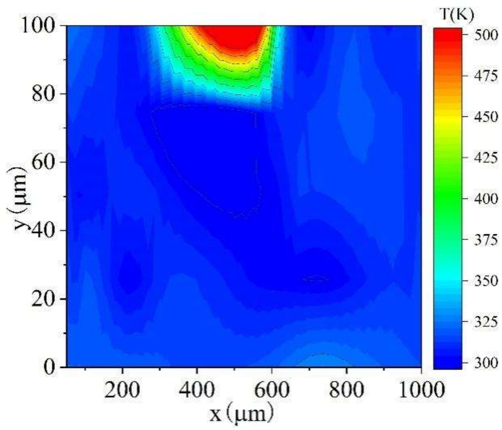

(a)1um

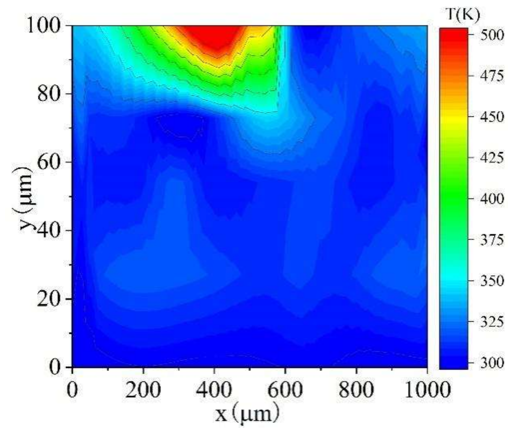

(b)8um

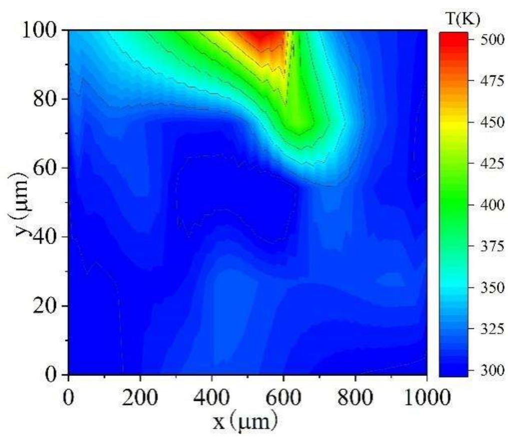

(c)15um

Fig. 4. Temperature distribution of different GaN thicknesses

The results of the computational efficiency and accuracy analysis are shown in Fig. 5, where (a) ~ (b) are the computational time comparison graph and absolute error comparison, respectively. Figure (a) exhibits that under the condition of the same accuracy with the LBM method, the method of this paper proposed in this study can significantly improve the computational efficiency, specifically, the computational efficiency is improved by about 33 times. And from the comparison of Fig. (b), it can be seen that this paper's method maintains a high computational accuracy with a maximum error of only about 1.2% compared with the LBM method. Compared with the macroscopic FDM method, the error of this paper's method is significantly smaller (the maximum error of FDM is about 9.3%), especially in the case of the enhanced power of the heat source.

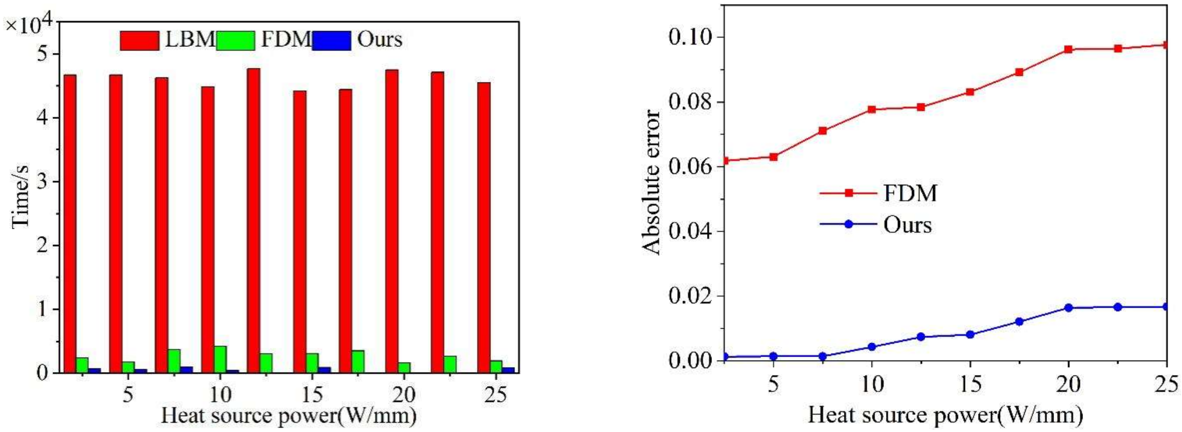

(a)Calculate the time comparison chart (b)Absolute error contrast

Fig. 5. Calculation efficiency and precision analysis results

4.1.3. Heat source spacing impact analysis. The device temperature distribution curves at different heat source spacings are shown in Fig. 6. The variation of the maximum temperature of the GaN device when the heat source spacing is increased from 50um to 70um. As the heat source spacing increases, the mutual thermal interference between the heat sources gradually decreases, resulting in a decrease in the maximum temperature of the device. This phenomenon reflects the importance of heat source spacing for device temperature control, especially when designing dense microelectronic devices, where proper heat source spacing can effectively reduce the thermal risk of the device. For all GaN layer thicknesses examined, the maximum temperature of the devices shows a clear decreasing trend with increasing heat source spacing. Especially in the case of thinner GaN layer thickness (e.g., 1 um), the effect of heat source spacing on the maximum temperature is more significant. This finding emphasizes that in the design of high power density electronic devices, the reasonable setting of heat source spacing is a key factor in optimizing the thermal performance of the device and improving the stability of the device. Reasonable selection of heat source spacing not only reduces the thermal interference between devices, but also significantly lowers the operating temperature of the device, which is of great practical significance for improving the heat transfer performance of high-temperature devices.

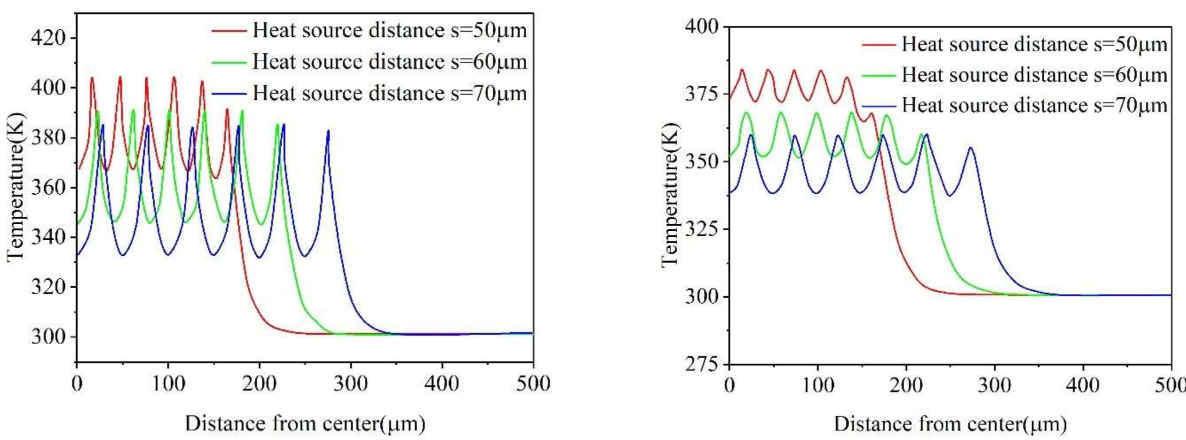

(a)1um (b)8um

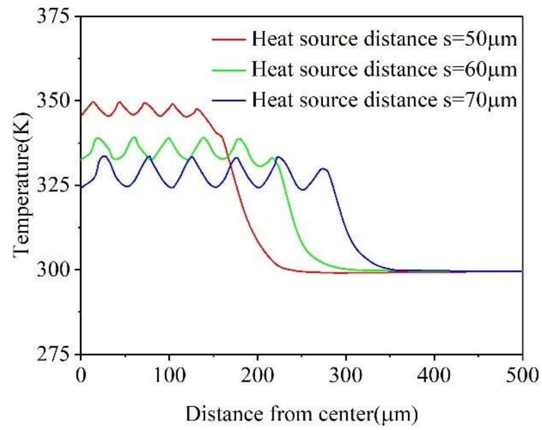

(c)15um

Fig. 6. Device temperature distribution curve at different heat source spacing

4.2. Simulation and analysis of nonlinear partial differential equations for heat transfer

4.2.1. Analysis of nonlinear partial differential equation solutions for heat transfer. Fig. 7 shows a three-dimensional image simulated by simulation software based on the numerical solution of the nonlinear partial differential equation for heat transfer, reflecting the relationship between time, temperature and thickness. Figure 8 reflects the comparison between the numerical solution of the heat transfer nonlinear partial differential equation as well as the actual data, where line 1 represents the actual data and line 2 represents the numerical solution of the heat transfer nonlinear partial differential equation. From Fig. 8, we can see that the numerical solution of the heat transfer nonlinear partial differential equation and the actual data are close to each other in the early stage, but with the passage of time, the offset gradually increases, because there is no influence on the structural parameters of the device material in terms of the porosity, pore radius, etc., heat and moisture transfer, and the physical parameters such as the diffusion of water vapor, etc. in the heat transfer nonlinear partial differential equation, and the temperature is constantly increasing with the passage of time In the high-temperature state, the above factors have a greater impact on the temperature reduction, therefore, as the temperature rises, the temperature calculated using the heat transfer nonlinear partial differential equation will be lower than the actual temperature, the reason is that the parameters of the device there is a small gap in the acceptable range of the results of the study, the results are very good to reveal the change rule of the temperature in the process of high-temperature device heat transfer.

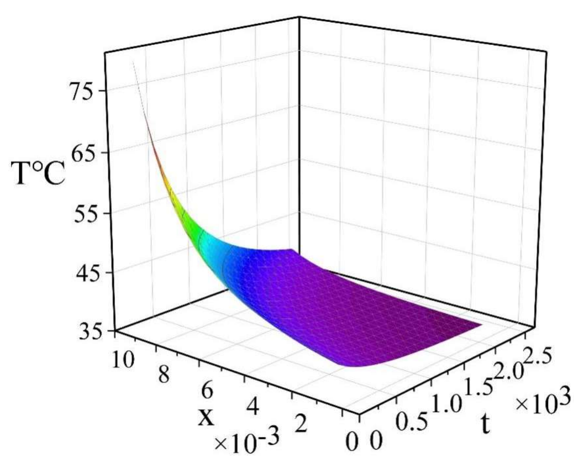

Fig. 7. Numerical solutions of nonlinear partial differential equations

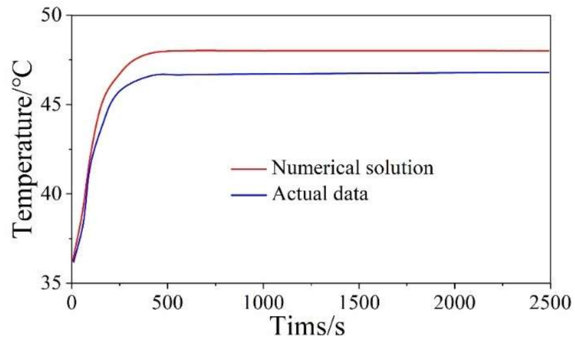

Fig. 8. Data comparison chart

4.2.2. Simulation and analysis of three types of heat transfer. In this subsection, the finite element results of the heat transfer of high temperature devices are simulated and analyzed, and it is known from the above that the heat transfer methods include heat conduction, heat convection and heat radiation, and the temperature changes in the heat transfer process of high temperature devices at different moments can be obtained, and the results of the three kinds of heat transfer simulation and analysis are shown in Fig. 9, in which (a)~(c) represent heat conduction, heat convection and heat radiation, respectively. The three graphs respectively show the changes in device temperature with time for different heat transfer methods, and it can be seen from the graphs that the temperature changes in the experiment have a good correlation with the simulated temperature changes. Figure 9(a) shows the comparison curve between the simulated and experimental values of the heat transfer of high-temperature devices, which shows that the temperature of the high-temperature device increases with the prolongation of time, and finally stabilizes at 49.93℃. Figure 9 (b) shows the comparison curve between the simulated and experimental values of heat convection of high temperature devices, it can be observed that with the extension of time, the temperature of high temperature devices increases and then decreases, and finally stabilized at 37.92 ℃. Fig. 9(c) shows the comparison curve between the simulated and experimental values of thermal radiation of the high temperature device, and it is observed that with the extension of time, the temperature of the high temperature period firstly increases and then decreases, and the rate of temperature increase and decrease is higher than that of the simulation process with simulation time of 10min and 20min. Observation of the three graphs shows that the temperature reached an equilibrium value in about ten minutes, and then with the extension of time, the temperature began to decline, this is due to the high temperature device temperature with the increase in time, the temperature is gradually decreasing, due to the temperature drop, resulting in a decrease in the temperature difference propulsion, the rate of heat transfer decreases, and the temperature of the outer surface decreases with it. The relative errors of the three simulations are 2.267%, 2.675% and 7.56% respectively. It can be seen that the simulation and analysis method in this paper accurately reflects the temperature change in the heat transfer process of the high temperature device.

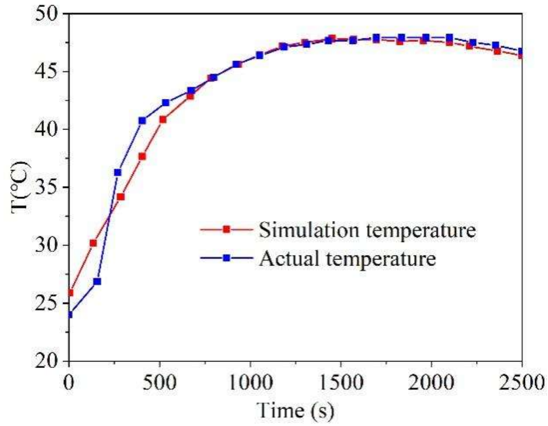

(a)Heat conduction

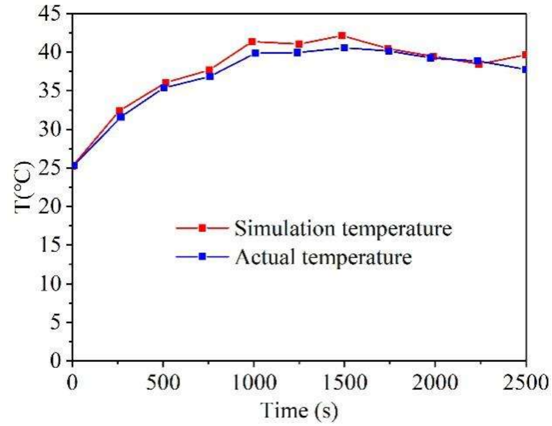

(b)Thermal convection

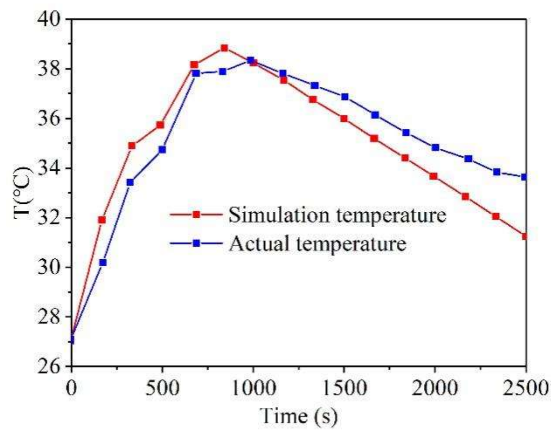

(c)Thermal radiation

Fig. 9. Three kinds of heat transfer simulation analysis

5. Conclusion

In this paper, according to the structural characteristics of high-temperature devices, using the appropriate instruments to obtain high-temperature device materials, integrated nonlinear partial differential equations, numerical simulation software, together with numerical simulation simulation analysis of the heat transfer characteristics of the research samples.

1) In the heat transfer process, when the thickness of the device is increasing, the temperature shows a tendency to decrease and then increase, and the temperature of the high-temperature device reaches a minimum when the layer thickness rises to 6.13 μm.

2) Among the three modes of heat transfer, the time of action and the temperatures of heat conduction, heat convection, and heat radiation all show a tendency to increase and then decrease, with the temperature of heat radiation changing most significantly.

Funding

This work was supported by Henan Province Science and Technology Key Project (No. 252102220112); the National Natural Science Foundation of China for the Youth Science Fund Project (No. 12204305).

References

[1] Andreeva, T. A., Bykov, N. Y., Gataulin, Y. A., Hvatov, A. A., Klimova, A. K., Lukin, A. Y., & Maslyaev, M. A. (2023). Methods of Partial Differential Equation Discovery: Application to Experimental Data on Heat Transfer Problem. Processes, 11(9), 2719.

[2] Delouei, A. A., Emamian, A., Ghorbani, S., & He, F. (2024). Spherical partial differential equation with non-constant coefficients for modeling of nonlinear unsteady heat conduction in functionally graded materials. ZAMM-Journal of Applied Mathematics and Mechanics/Zeitschrift für Angewandte Mathematik und Mechanik, e202300725.

[3] Cuesta, F. J., & Álvarez, M. D. (2017). Mathematical modeling for heat conduction in stone fruits. International Journal of Refrigeration, 80, 120-129.

[4] Gao, X. W., Huang, S. Z., Cui, M., Ruan, B., Zhu, Q. H., Yang, K., ... & Peng, H. F. (2017). Element differential method for solving general heat conduction problems. International Journal of Heat and Mass Transfer, 115, 882-894.

[5] Choi, S., Lee, H., Ghaffari, R., Hyeon, T., & Kim, D. H. (2016). Recent advances in flexible and stretchable bio-electronic devices integrated with nanomaterials. Advanced materials, 28(22), 4203-4218.

[6] Stassen, I., Burtch, N., Talin, A., Falcaro, P., Allendorf, M., & Ameloot, R. (2017). An updated roadmap for the integration of metal–organic frameworks with electronic devices and chemical sensors. Chemical Society Reviews, 46(11), 3185-3241.

[7] Almubarak, A. A. (2017). The effects of heat on electronic components. Int. J. Eng. Res. Appl, 7(5), 52-57.

[8] McCluskey, F. P., Podlesak, T., & Grzybowski, R. (2018). High temperature electronics. CRC press.

[9] Šiškins, M., Mullan, C., Son, S. K., Yin, J., Watanabe, K., Taniguchi, T., ... & Mishchenko, A. (2019). High-temperature electronic devices enabled by hBN-encapsulated graphene. Applied Physics Letters, 114(12).

[10] Lin, X., Salari, M., Arava, L. M. R., Ajayan, P. M., & Grinstaff, M. W. (2016). High temperature electrical energy storage: advances, challenges, and frontiers. Chemical Society Reviews, 45(21), 5848-5887.

[11] He, Z., Yan, Y., & Zhang, Z. (2021). Thermal management and temperature uniformity enhancement of electronic devices by micro heat sinks: A review. Energy, 216, 119223.

[12] Li, Q., Yao, F. Z., Liu, Y., Zhang, G., Wang, H., & Wang, Q. (2018). High-temperature dielectric materials for electrical energy storage. Annual Review of Materials Research, 48(1), 219-243.

[13] Razeeb, K. M., Dalton, E., Cross, G. L. W., & Robinson, A. J. (2018). Present and future thermal interface materials for electronic devices. International Materials Reviews, 63(1), 1-21.

[14] Wang, C., Wang, Y., Chen, Y., Gao, W., Xu, Q., Wang, Z., ... & Zhong, J. (2019). Coupling model and electronic compensation of antenna-radome system for hypersonic vehicle with effect of high-temperature ablation. IEEE Transactions on Antennas and Propagation, 68(3), 2340-2355.

[15] Hota, S. S., Panda, D., & Choudhary, R. N. P. (2024). Structural, dielectric, electrical, and leakage current properties of SrWO4 for electronic devices. Journal of the Korean Ceramic Society, 61(6), 1207-1221.

[16] Meng, X., Zhang, M., Duan, K., Zheng, X., Zhai, Y., Feng, S., & Zhang, Y. (2023). Research on transient temperature rise measurement method for semiconductor devices based on photothermal reflection. IEEE Transactions on Instrumentation and Measurement, 72, 1-9.

[17] Abdulrahman B M Alzahrani. (2025). Solving the fractional nonlinear dispersive K(m, n, 1) partial differential equation: techniques and applications. Physica Scripta(3),035215-035215.

[18] Attiya Nazneen,Rashid Nawaz,Laiq Zada,Nasir Ali,Mohamed Benghanem & Hijaz Ahmad. (2025). Analysis of the non-linear higher dimensional fractional differential equations arising in dusty plasma using the Atangana–Baleanu fractional derivative. Results in Engineering104116-104116.

[19] Hayman Thabet,Subhash Kendre & James Peters. (2025). Numerical solutions for space–time conformable nonlinear partial differential equations via a scientific machine learning technique. Neurocomputing129134-129134.

[20] Luqman Khaleel Hyder Alatrushi,Mohammad Takey Elias Kassim,Emad Toma Karash & Waleed Mohammed Najm. (2024). The Effect of Changing the Reinforcing Angle of a Composite Material on the Tensile and Compressive Resistance Using the ANSYS Program. Annales de Chimie - Science des Matériaux(5),

[21] Haoqing Kang,Jian Gao,Shicong Wang,Kanglei Zhou & Chuanyi Huang. (2024). Research on Stability of Tower Crane based on ANSYS Software. Frontiers in Computing and Intelligent Systems(3),74-79.